https://doi.org/10.5194/tc-2021-37
Preprint. Discussion started: 2 February 2021

The Cryosphere Discussions

Indication of high basal melting at EastGRIP drill site on the Northeast Greenland Ice Stream

Ole Zeising[1,2] and Angelika Humbert[1,2]

[1]Alfred-Wegener-Institut Helmholtz-Zentrum für Polar- und Meeresforschung, Bremerhaven, Germany
[2]University of Bremen, Department of Geosciences, Germany

Correspondence: Ole Zeising (ole.zeising@awi.de)

Abstract. The accelerated ice flow of ice streams that reach far into the interior of the ice sheet, is associate with lubrication of the ice sheet base by basal melt water. However, the amount of basal melting under the large ice streams – such as the Northeast Greenland Ice Stream (NEGIS) – are largely unknown. In-situ measurements of basal melt rates are important from various perspectives as they indicate the heat budget, the hydrological regime and the role of sliding in glacier motion. The few previous estimates of basal melt rates in the NEGIS region were $0.1\,\mathrm{m\,a^{-1}}$ and more, based on radiostratigraphy methods. These finding raised the question of the heat source, since even an increased geothermal heat flux could not deliver the necessary amount of heat. Here, we present basal melt rates at the recent deep drill site EastGRIP, located in the center of NEGIS. Within two subsequent years, we found basal melt rates of $(0.16 - 0.22) \pm 0.01\,\mathrm{m\,a^{-1}}$, that are based on analysis of repeated phase-sensitive radar measurements. In order to quantify the contribution of processes that cause a heat flux into the ice, we carried out an assessment of the energy sources and found the subglacial water system to play a key role in facilitating such high melt rates.

1 Introduction

Ice sheet models are used to quantify the contribution of the Greenland Ice Sheet (GrIS) to future sea-level rise under different climatic scenarios. The distinctive extent of Greenland's largest ice stream – the Northeast Greenland Ice Stream (NEGIS, Fig. 1) – can only be represented well if an higher-order approximation is considered for the momentum balance and initial states are based on inversion (Goelzer et al., 2018). Primarily, this is due to the model's ability to accurately represent lubrication and thus the subsequent sliding at the ice stream base that occurs.

The NEGIS is the only large ice stream in Greenland, extending from a distance of 100 km from the ice divide over a length of about 700 km towards the coast (Fahnestock et al., 1993, 2001b; Joughin et al., 2001). It drains about 12 % of Greenland's ice through three major outlet glaciers Nioghalvfjerdsbrae, Zachariæ Isstrøm and Storstrømmen Glacier (Rignot and Mouginot, 2012). Loss of the floating tongue of Zachariæ Isstrøm has already led to acceleration and mass loss (Mouginot et al., 2015). Consequently, it is expected and projected that NEGIS will contribute significantly to sea level rise in the future (Khan et al., 2014), highlighting the importance to understand its lubrication.

One hypothesis for the genesis of NEGIS is locally increased basal melt rates at the onset area that enable basal sliding as basal melt water forms a subglacial hydrological system (Fahnestock et al., 2001a; Christianson et al., 2014; Franke et al.).

https://doi.org/10.5194/tc-2021-37
Preprint. Discussion started: 2 February 2021

The Cryosphere Discussions
Open Access
EGU

However, little is known about the amount of subglacial water system below the $2000 - 3000\,\mathrm{m}$ thick ice sheet. First estimates of basal melt rates by Fahnestock et al. (2001a) and later by MacGregor et al. (2016) are based on the interpretation of chronology in radiostratigraphy. Both studies found melt rates of $0.1\,\mathrm{m\,a^{-1}}$ and more – which is extremely large for inland ice. The cause for such intensive melt was attributed to a high geothermal heat flux which possibly originates from a remnant of the passing of the Icelandic hot spot (Fahnestock et al., 2001a; Rogozhina et al., 2016; Martos et al., 2018; Alley et al., 2019). In order to conduct, among other things, direct observations of flow regimes and basal conditions of ice streams, an ice core is drilled in the course of the East Greenland Ice-Core Project (EastGRIP) near the onset of the NEGIS. Here, surface velocities reach about $57\,\mathrm{m\,a^{-1}}$ (Hvidberg et al., 2020) and the NEGIS widens (Fig. 1). Smith-Johnsen et al. (2020) forced an ice model with a locally increased geothermal heat fluxes below the EastGRIP drill site and found that a heat flux of $0.97\,\mathrm{W\,m^{-2}}$ (corresponding to a basal melting rate of $0.1\,\mathrm{m\,a^{-1}}$ (Fahnestock et al., 2001a)) is necessary to reasonably reproduce the velocities of NEGIS.

However, measurements with an adequate accuracy are still required to narrow down the basal melt rates further. Here, we present the first estimates of basal melting rates from repeated in-situ phase-sensitive radar measurements from the EastGRIP drill site.

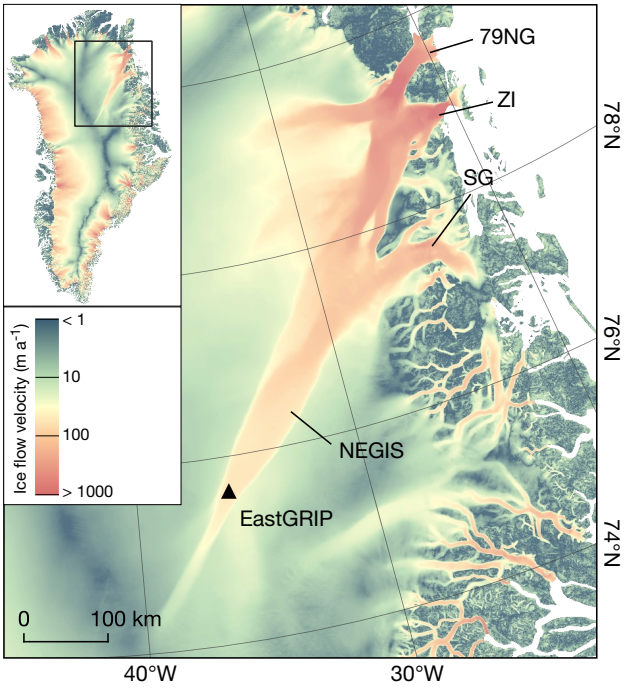

Figure 1. Surface ice flow velocity map of the Greenland Ice Sheet (Joughin et al., 2018). The box in the overview map (upper left corner) marks the boundaries of the main figure showing northeast Greenland and the Northeast Greenland Ice Stream (NEGIS), which drains into the three major outlet glaciers, namely Nioghalvfjerdsbrae (79°N Glacier, 79NG), Zachariæ Isstrøm (ZI) and Storstrømmen Glacier (SG). The location of the EastGRIP drill site is denoted by the black triangle.

https://doi.org/10.5194/tc-2021-37
Preprint. Discussion started: 2 February 2021


The Cryosphere Discussions
Open Access
EGU

2 Data and Methods

2.1 Data

We deployed an autonomous phase-sensitive radio-echo sounder (ApRES; Brennan et al., 2014; Nicholls et al., 2015) within a near surface trench at the EastGRIP drill site (Fig. 1). The radar performed a measurement once a day during winter from 08/2017 – 04/2018 and 08/2018 – 05/2019. Within a single measurement, the ApRES transmits a sequence of 100 chirps with a duration of 1 s in which the frequency of the transmitted electromagnetic wave is increased from 200 to 400 MHz.

2.2 Basal melting

The recorded ApRES time series allows for a precise estimation of vertical displacements of internal layers and of the basal reflector relative to the instrument from consecutive measurements. However, basal melt rates can not be derived directly, so other quantities that influence the measured ice thickness H need to be derived first. Here and in the following, the term 'measured ice thickness' is defined as the range between the ApRES and the ice base, which was determined using the depth of the basal return. The total ice thickness – the range from the surface to the ice base – is about 7 to $8\,\mathrm{m}$ thicker and includes the upper firn and snow layers.

A change in the measured ice thickness ΔH within the time interval Δt is caused by firn densification ΔH_f, by vertical strain $\Delta H_{\varepsilon_{zz}}$ and by basal melting ΔH_b (Nicholls et al., 2015):

$$\frac{\Delta H}{\Delta t} = \frac{\Delta H_f}{\Delta t} + \frac{\Delta H_{\varepsilon_{zz}}}{\Delta t} + \frac{\Delta H_b}{\Delta t}. \tag{1}$$

Thus, the basal melt rate a_b is defined as

$$a_b = \frac{\Delta H_b}{\Delta t}. \tag{2}$$

In contrast to the total ice thickness, the change in the measured ice thickness is not affected by accumulation and only by the densification occurring below the radar instrument.

The thickness change due to vertical strain is the integral over the entire vertical column of the vertical strain component ε_{zz}

$$\Delta H_{\varepsilon_{zz}} = \int_0^H \varepsilon_{zz}(z)\,\mathrm{d}z. \tag{3}$$

Vertical strain is defined as the vertical gradient of the vertical displacement component $u_z(z)$

$$\varepsilon_{zz}(z) = \frac{\partial u_z(z)}{\partial z}. \tag{4}$$

All three quantities ΔH, ΔH_f and $\Delta H_{\varepsilon_{zz}}$ are described by vertical displacements and hence by the measurement itself in a consistent manner. ΔH is derived from the vertical displacement of the basal return. As densification processes are limited in depth, ΔH_f can be estimated based on the vertical displacement of the layers within the ice. In order to estimate $\Delta H_{\varepsilon_{zz}}$, the

https://doi.org/10.5194/tc-2021-37
Preprint. Discussion started: 2 February 2021


The Cryosphere Discussions

vertical displacement of layers above the noise-level depth limit h (depth at which the noise-level of the ApRES measurement prevents an unambiguous estimation) needs to be analyzed and extrapolated to the ice base. The vertical gradient of the vertical displacement is the vertical strain.

2.3 ApRES processing

In order to derive amplitude- and phase-depth profiles for the ApRES signal processing, we followed the processing described by Brennan et al. (2014), Nicholls et al. (2015) and Stewart et al. (2019). For the conversion from travel time to depth, we used a vertical propagation velocity of $168,194\,\mathrm{km\,s^{-1}}$ according to relative permittivity of $\epsilon_r = 3.15$. To derive vertical displacements of layers within the ice as well as for the basal return from the ApRES time series, we used a modification of the process described by Vaňková et al. (2020). Both methods are based on estimated phase differences derived from cross-correlation of individual depth segments. In contrast to Vaňková et al. (2020), we compare the first measurement with each repeated measurement instead of pairwise time-consecutively measurements to reduce measurement errors. Here, the ApRES time series is used to achieve a reliable estimation of the annual mean basal melt rate.

First, we divided the depth profile into 6 m wide range segments with a 3 m overlap from a depth of 20 m below the antennas to 20 m above the ice base and a wider segment of 10 m (-9 to +1 m) around the basal return, characterized by a strong increase in amplitude. Each depth segment of the first measurement (t_1) was cross-correlated with the same segment of each repeated measurements (t_i). The lag of the minimum mean phase difference obtained from the cross-correlation gives the cumulative displacement at the given depth. The range of expected lag was limited by the estimation to the previous measurement (t_1 – t_{i-1}). This results in a time series of displacements for each segment individually. The vertical displacement of the basal segment is the change in the measured ice thickness ΔH. Segments whose time series contain outliers or whose shift deviates significantly from their neighboring segments were discarded. Next, we estimate the vertical strain $\varepsilon_{zz}^{\mathrm{obs}}$ as described in Equation (4) and quantify ΔH_f as well as $\Delta H_{\varepsilon_{zz}}$. We found a linear fit $u_z(z)$ to match the curve of the cumulative vertical displacements of the remaining segments within the ice (below a depth of 250 m to exclude layers affected by firn densification) best

$$u_z(z) = \varepsilon_{zz}^{\mathrm{obs}} \cdot z + \Delta H_f, \quad 250\,\mathrm{m} \leq z \leq h \tag{5}$$

The gradient of this fit is $\varepsilon_{zz}^{\mathrm{obs}}$ and the offset at the surface is ΔH_f. However, ε_{zz} for $z \geq h$ is unknown. Here, we used two scenarios in order estimate a range $\Delta H_{\varepsilon_{zz}}$ and provide a comparison to another often considered scenario (Appendix Fig. A1). First, we assumed that ε_{zz} is constant with depth:

$$\varepsilon_{zz}^{\mathrm{const}}(z) = \varepsilon_{zz}^{\mathrm{obs}}, \quad 0 \leq z \leq H \tag{6}$$

As a second scenario, we used a vertical strain distribution ($\varepsilon_{zz}^{\mathrm{sim}}$) obtained from an ice sheet model based on inverse surface flow velocities (Rückamp et al., 2020). Here, $\varepsilon_{zz}^{\mathrm{sim}}$ increases with depth and reaches values of roughly twice $\varepsilon_{zz}^{\mathrm{obs}}$ at the base. For comparison, we also used a Dansgaard–Johnsen distribution of the vertical strain (Dansgaard and Johnsen, 1969), despite no-slip at the base is likely unrealistic (MacGregor et al., 2016). This assumes a constant $\varepsilon_{zz}^{\mathrm{dj}}$ from the surface to the depth at which the uniform horizontal velocity changes to shear flow. From here, the vertical strain-rate decreases linearly to zero. As

https://doi.org/10.5194/tc-2021-37
Preprint. Discussion started: 2 February 2021

The Cryosphere Discussions
Open Access
EGU

the depth of increased shear flow at EastGRIP is yet unknown, we assume that shear flow is occurring from the noise-level depth limit (h) on, in order to underestimate $\Delta H_{\varepsilon_{zz}}$ and thus to overestimate the basal melt rate:

$$\varepsilon_{zz}^{\mathrm{dj}}(z) = \begin{cases} \varepsilon_{zz}^{\mathrm{obs}} & 0 \le z \le h \\ \varepsilon_{zz}^{\mathrm{obs}} \left(1 - \frac{h-z}{h-H}\right) & h < z \le H \end{cases} \tag{7}$$

In order to be less dependent on a single measurement, we averaged the annual mean values of $\varepsilon_{zz}^{\mathrm{obs}}$, ΔH_f and ΔH from the last 65 records (roughly 25 % of the measurements). Finally, $\Delta H_{\varepsilon_{zz}}$ was derived from Equation (3) for the two vertical strain distributions ($\Delta H_{\epsilon_{zz}}^{\mathrm{const}}$, $\Delta H_{\epsilon_{zz}}^{\mathrm{sim}}$), and the basal melt rate a_{b} from Equation (1). Given errors are based on the standard deviation of the estimates based on the considered 65 measurements and a 1 % uncertainty in the signal propagation speed in ice (Fujita et al., 2000). For visualization, we calculated the cumulative vertical displacement referenced to the ice bed.

3 Results

The analysis of the 2017/18 ApRES time series revealed a measured ice thickness (distance between radar and ice base) of roughly 2668 m at the EastGRIP drill site with an annual mean change of $-0.471\,\mathrm{m\,a^{-1}}$ (Tab. 1, Fig. 2). We derived a vertical strain of -0.068×10^{-3} from reliable estimates of vertical displacements feasible to a depth of 1450 m. The dynamic thinning of the ice derived from the two scenarios ranges from $-0.181\,\mathrm{m\,a^{-1}}$ ($\Delta H_{\epsilon_{zz}}^{\mathrm{dj}}$) to $-0.194\,\mathrm{m\,a^{-1}}$ ($\Delta H_{\epsilon_{zz}}^{\mathrm{sim}}$). The firn densification – the intercept of the linear fit at the surface (see Fig. 2) – occurring below the radar is $0.074\,\mathrm{m\,a^{-1}}$. This results in a basal melt rate between 0.203 and $0.216\,\mathrm{m\,a^{-1}}$. The numbers derived from the time series recorded in 2018/19 differs slightly (Tab. 1, Appendix Fig. A2). The annual mean change in measured ice thickness is 27 mm (or 6 %) less and the firn densification has increased by 15 mm (or 20 %). Thus, the basal melt rate varies from 0.160 to $0.173\,\mathrm{m\,a^{-1}}$ and are 27 % lower than the year before.

Table 1. Results for measured ice thickness change (ΔH), vertical strain (ε_{zz}), dynamic ice thickness change obtain from a constant vertical strain ($\Delta H_{\epsilon}^{\mathrm{const}}$) and based on a simulation ($\Delta H_{\epsilon}^{\mathrm{sim}}$), firn densification ($\Delta H_f$) and basal melting ($a_{\mathrm{b}}$) for both time series projected to 365 days.

Year	ΔH (m)	ε_{zz} ($\times 10^{-3}$)	$\Delta H_{\epsilon}^{\mathrm{const}}$ (m)	$\Delta H_{\epsilon}^{\mathrm{sim}}$ (m)	ΔH_f (m)	a_{b} ($\mathrm{m\,a^{-1}}$)
2017/18	-0.471 ± 0.008	-0.068 ± 0.001	-0.181 ± 0.001	-0.194 ± 0.001	-0.074 ± 0.001	$(0.203 - 0.216) \pm 0.008$
2018/19	-0.444 ± 0.006	-0.068 ± 0.002	-0.182 ± 0.005	-0.195 ± 0.005	-0.089 ± 0.002	$(0.160 - 0.173) \pm 0.011$

https://doi.org/10.5194/tc-2021-37
Preprint. Discussion started: 2 February 2021

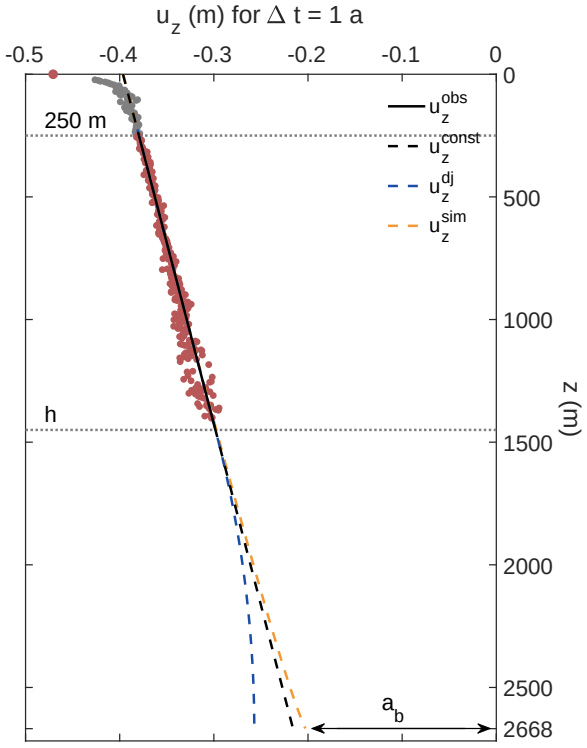

Figure 2. Derived vertical displacements u_z of the surface and selected internal layers referenced to the ice bed from 2017/18 ApRES time series. Derived displacements used for melt rate estimations are marked by red dots and of layers within the firn by gray dots. The estimated displacements between a depth of $250\,\mathrm{m}$ and h are used to calculate a linear fit (solid black line) which gradient is the vertical strain. Extrapolations to the bottom are shown by the dashed lines. The offset at the ice bed is caused by basal melting and the difference between the surface intercept of the linear fit and the derived surface displacement is the firn compaction.

4 Discussion

We used estimated vertical displacements from the upper half of the ice column to estimate the dynamic thinning, since noise prevents an unambiguous estimation of the vertical strain for the lower half. To cover a range of variations in the dynamic thinning, we used three different scenarios for vertical strain distribution. As the Dansgaard-Johnsen distribution describes a decrease in vertical velocity to zero at the ice base (representing a no-slip boundary condition), we do not consider this further. The vertical strain distribution obtained from the inverse ice sheet model is expected to give a more realistic representation. The resulting dynamic thinning of the simulated vertical strain and the constant strain differs only slightly. However, we cannot exclude that larger strain values are reached at the base, which would lead to an overestimation of the basal melt rates. In case of a non-existing melt rate, the dynamic thinning of the lower half of the ice column would be in average more than four times

https://doi.org/10.5194/tc-2021-37
Preprint. Discussion started: 2 February 2021


The Cryosphere Discussions

as large as of the upper half. However, a strong increase is not found in higher-order ice sheet simulations (Rückamp et al., 2020).

The derived vertical strain is based on more than 300 vertical displacements estimated between the firn-ice transition and about $1450\,\mathrm{m}$. In contrast, the estimation of the displacement of the basal return is based on the phase shift of only one segment around the basal return, slightly above the noise level. This makes the determination more prone to errors. Instead comparing the first measurement (t_1) with all repeated measurements (t_i), the pairwise comparison of time-consecutively measurements (t_{i-1} and t_i), as it is shown by Vaňková et al. (2020), leads to a lower thinning rate of ΔH in 2017/18 than in 2018/19 ($-0.441 \pm 0.004\,\mathrm{m\,a^{-1}}$ in 2017/18, $-0.467 \pm 0.009\,\mathrm{m\,a^{-1}}$ in 2018/19). Thus, the variability found is not necessarily a variability of the ice sheet system but can rather be influenced by the methodology.

A variation in the selected depth limit of densification, to exclude segments affected by densification, causes slight changes in vertical strain and thus in basal melt rate in the order of millimeters. However, we observed an increased densification rate within the considered 65 records. The increased densification can possibly be a result of increased load from the camp at the surface.

Our derived basal melt rates of 0.16 to $0.22\,\mathrm{m\,a^{-1}}$ are slightly above previous estimates from airborne radar measurements. Fahnestock et al. (2001a) and MacGregor et al. (2016) found melt rates in the order of $0.1\,\mathrm{m\,a^{-1}}$ in the vicinity of the EastGRIP drill side, but larger melt rates of $> 0.15\,\mathrm{m\,a^{-1}}$ further upstream in the onset region of NEGIS. Both studies used a constant vertical strain over depth where basal melting occurs. Smith-Johnsen et al. (2020) found that basal melt rates of $0.1\,\mathrm{m\,a^{-1}}$, derived from a heat flux of $0.97\,\mathrm{W\,m^{-2}}$, are needed at the location of the EastGRIP drill site to reproduce the NEGIS in an ice sheet model.

4.1 Considerations of the energy balance at the ice base

In order to constrain the heat flux required to sustain the basal melt rates a_b derived in this study, we consider the energy balance at the ice base. As for any surface across which a physical quantity may not be continuous, a jump condition is formulated. In typical continuum mechanical formulation, the jump ($[\![\psi]\!]$) of a quantity ψ is defined as $[\![\psi]\!] = \psi^+ - \psi^-$, meaning the difference in the quantity ψ across the interface (Greve and Blatter, 2009). The jump condition of the energy at the ice base reads as

$$[\![\boldsymbol{q}\cdot\boldsymbol{n}]\!] - [\![\boldsymbol{v}\cdot\mathbf{t}\cdot\boldsymbol{n}]\!] + [\![\rho\left(u+\tfrac{1}{2}\boldsymbol{v}^2\right)(\boldsymbol{v}-\boldsymbol{w})\cdot\boldsymbol{n}]\!] = [\![\boldsymbol{q}\cdot\boldsymbol{n}]\!] - [\![\boldsymbol{v}\cdot\mathbf{t}\cdot\boldsymbol{n}]\!] + \rho_\mathrm{i}\,a_\mathrm{b}\,[\![u]\!] = 0 \tag{8}$$

with the heat flux q, the velocity $\boldsymbol{v}$, the velocity of the singular surface $\mathbf{w}$, the normal vector $\boldsymbol{n}$ pointing outwards of the ice body, the Cauchy stress $\mathbf{t}$ and the internal energy u (Greve and Blatter, 2009). The jump of the heat flux $[\![\boldsymbol{q}\cdot\boldsymbol{n}]\!]$ becomes $(\boldsymbol{q}_\mathrm{geo}+\boldsymbol{q}_\mathrm{sw})\cdot\boldsymbol{n}-\kappa(T)\,\mathrm{grad}\,T$, with $\boldsymbol{q}_\mathrm{geo}$ the geothermal heat flux and $\boldsymbol{q}_\mathrm{sw}$ the heat flux from subglacial water with a temperature above pressure melting point, T temperature and κ thermal conductivity. For the jump in work of surface forces we find

$$[\![\boldsymbol{v}\cdot\mathbf{t}\cdot\boldsymbol{n}]\!] = \boldsymbol{v}^\mathrm{sw}\cdot\mathbf{t}^\mathrm{sw}\cdot\boldsymbol{n} - \boldsymbol{v}_\mathrm{b}^\mathrm{i}\cdot\mathbf{t}^\mathrm{i}\cdot\boldsymbol{n} \tag{9}$$

https://doi.org/10.5194/tc-2021-37
Preprint. Discussion started: 2 February 2021


The Cryosphere Discussions
Open Access
EGU

with $\mathbf{t}^{\mathrm{sw}}$ the Cauchy stress of the subglacial water side of the singular surface, $\boldsymbol{v}_{\mathrm{b}}^{\mathrm{i}}$ the ice velocity and $\mathbf{t}^{\mathrm{i}}$ the stress field of the ice at the base.

We split the traction vector of the subglacial water in a normal and tangential component, with the water pressure p_{w} the stress in the normal direction and use for the tangential component an empirical relation

$$\mathbf{t}^{\mathrm{sw}} \cdot \boldsymbol{n} = -p_{\mathrm{w}} \boldsymbol{n} + C^{\mathrm{i/sw}} \rho_{\mathrm{w}} |\boldsymbol{v}^{\mathrm{sw}}|^2 \boldsymbol{e}_{\mathrm{t}} \tag{10}$$

with $\boldsymbol{e}_{\mathrm{t}} = \boldsymbol{v}^{\mathrm{sw}}/|\boldsymbol{v}^{\mathrm{sw}}|$ and $\boldsymbol{e}_{\mathrm{t}} \perp \boldsymbol{n}$. The roughness at the underside of the ice is $C^{\mathrm{i/sw}}$, similar as a Manning roughness is taken into account in subglacial conduits. So that the part of the subglacial water becomes

$$\boldsymbol{v}^{\mathrm{sw}} \cdot \mathbf{t}^{\mathrm{sw}} \cdot \boldsymbol{n} = -p_{\mathrm{w}} \boldsymbol{v}^{\mathrm{sw}} \cdot \boldsymbol{n} + \boldsymbol{v}^{\mathrm{sw}} \cdot C^{\mathrm{i/sw}} \rho_{\mathrm{w}} |\boldsymbol{v}^{\mathrm{sw}}|^2 \boldsymbol{e}_{\mathrm{t}} = -p_{\mathrm{w}} \boldsymbol{v}_{\perp}^{\mathrm{sw}} + C^{\mathrm{i/sw}} \rho_{\mathrm{w}} |\boldsymbol{v}_{\shortparallel}^{\mathrm{sw}}|^3 \tag{11}$$

with $\boldsymbol{v}_{\perp}^{\mathrm{sw}}, \boldsymbol{v}_{\shortparallel}^{\mathrm{sw}}$ the normal and tangential velocity of the subglacial water, respectively. This formulation is quite similar to the treatment of the jump condition at an ice shelf base. For the traction vector at the ice base, we follow the same procedure and find

$$\mathbf{t}^{\mathrm{i}} \cdot \boldsymbol{n} = -N \boldsymbol{n} + \tau_{\mathrm{b}} \boldsymbol{e}_{\mathrm{t}} \tag{12}$$

with N the normal component and τ_{b} the component in the tangential plane. For $\boldsymbol{v}_{\mathrm{b}}^{\mathrm{i}} \cdot \mathbf{t}^{\mathrm{i}} \cdot \boldsymbol{n}$ we find

$$\boldsymbol{v}_{\mathrm{b}}^{\mathrm{i}} \cdot \mathbf{t}^{\mathrm{i}} \cdot \boldsymbol{n} = -N \boldsymbol{v}_{\mathrm{b}}^{\mathrm{i}} \cdot \boldsymbol{n} + \tau_{\mathrm{b}} \boldsymbol{v}_{\mathrm{b}}^{\mathrm{i}} \cdot \boldsymbol{e}_{\mathrm{t}} \tag{13}$$

With the jump of the internal energy $[\![u]\!] = L$, we are can reformulate Eq. (8) to

$$q_{\mathrm{geo}}^{\perp} + q_{\mathrm{sw}}^{\perp} = \rho_{\mathrm{i}} a_{\mathrm{b}} L + \kappa(T) \operatorname{grad} T - p_{\mathrm{w}} \boldsymbol{v}_{\perp}^{\mathrm{sw}} + C^{\mathrm{i/sw}} \rho_{\mathrm{w}} |\boldsymbol{v}_{\shortparallel}^{\mathrm{sw}}|^3 + N \boldsymbol{v}_{\mathrm{b}}^{\mathrm{i}} \cdot \boldsymbol{n} - \tau_{\mathrm{b}} \boldsymbol{v}_{\mathrm{b}}^{\mathrm{i}} \cdot \boldsymbol{e}_{\mathrm{t}} \tag{14}$$

The tangential components $C^{\mathrm{i/sw}} \rho_{\mathrm{w}} |\boldsymbol{v}_{\shortparallel}^{\mathrm{sw}}|^3$ and $\tau_{\mathrm{b}} \boldsymbol{v}_{\mathrm{b}}^{\mathrm{i}} \cdot \boldsymbol{e}_{\mathrm{t}}$ are frictional heating and are dominating the contribution of heat arising from work of surface forces. They need to be seen as two end members of the system: either the ice is only in contact with a vertically extensive subglacial hydrological system, then $C^{\mathrm{i/sw}} \rho_{\mathrm{w}} |\boldsymbol{v}_{\shortparallel}^{\mathrm{sw}}|^3$ is at place, or the subglacial hydrological system is permanently in contact with a lubricated base, then the second term $\tau_{\mathrm{b}} \boldsymbol{v}_{\mathrm{b}}^{\mathrm{i}} \cdot \boldsymbol{e}_{\mathrm{t}}$ is governing.

Next, we aim at constraining the individual terms for which we use the following material parameters: $\rho_{\mathrm{i}} = 910\,\mathrm{kg\,m^{-3}}$, the latent heat of fusion, $L = 335\,\mathrm{kJ\,kg^{-1}}$, and the thermal conductivity for ice at $273.15\,\mathrm{K}$ $\kappa(273.15\,\mathrm{K}) = 2.07\,\mathrm{W\,m^{-1}\,K^{-1}}$ (Greve and Blatter, 2009).

We consider three scenarios: (i) there is only temperate ice that is melting, (ii) heat is required to warm the ice to the pressure melting point and (iii) friction at the base is contributing significantly to melt rate. (i) For temperate ice and no heat arising from work of surface forces we find a melt rates of at least $0.16\,\mathrm{m\,a^{-1}}$ to correspond to a heat flux of $1.56\,\mathrm{W\,m^{-2}}$. (ii) Considering $\operatorname{grad} T$ to be between 10^{-1} and $10^{-3}\,\mathrm{m\,a^{-1}}$ raises the required heat flux into the ice by 0.207 to $0.0207\,\mathrm{W\,m^{-2}}$.

(iii) Heat arising from work of the surface forces may, however, reduce the required heat flux into the ice to melt this amount of ice. To this end, we need to estimate the magnitude of the components of the stress tensors.

https://doi.org/10.5194/tc-2021-37
Preprint. Discussion started: 2 February 2021

The Cryosphere Discussions
Open Access
EGU

We assume that the normal stress component N is hydrostatic and bridging stresses to be negligible. With a mean density of ice of $910\,\mathrm{kg\,m^{-3}}$ we find $N = 23.8\,\mathrm{MPa}$. The normal velocity is of the order of the basal melt rate $v_\mathrm{b}^\perp \approx 0.2\,\mathrm{m\,a^{-1}}$ by assuming the velocity of the interface ($\boldsymbol{w}$) to be zero. The normal component of the ice side is then in the order of $0.15\,\mathrm{W\,m^{-2}}$. For the tangential components of the ice side, we consider the shear stress at the base to be $\tau_\mathrm{b} \approx 1$ to $100\,\mathrm{kPa}$. This compares to basal shear stress found by Rückamp et al. (2020) of 50 kPa. To constrain the sliding velocity we assume it to be maximum the surface velocity and minimum half of the surface velocity. This leads to a tangential component on the ice side to be up to $150\,\mathrm{mW\,m^{-2}}$ (Fig. 3).

Next, we constrain the normal component of the subglacial water $p_\mathrm{w}\boldsymbol{v}_\perp^\mathrm{sw}$. A water pressure of 10 to $23\,\mathrm{MPa}$ is consistent with subglacial hydrological modelling. Assuming the normal velocity to be at most as large as the basal melt rate, we find the range of this term to be between 51 to $116\,\mathrm{mW\,m^{-2}}$ (Fig. 3). The tangential component $C^\mathrm{i/sw}\rho_\mathrm{w}|\boldsymbol{v}_\shortparallel^\mathrm{sw}|^3$ needs an assumption on the roughness $C^\mathrm{i/sw}$, for which we consider a range from the roughness of the ice shelf base to maximum a ten times larger than this 10^{-3} to 10^{-2}. The motivation for this is that ice shelf roughness is governed by convection cells at the interface, whereas in the inland ice, the interaction with the bedrock may lead to a larger roughness. As nothing is known about the shape of the subglacial conduit, the range of velocity cannot be constrained well. We consider a similar speed like the ocean $0.1\,\mathrm{m\,s^{-1}}$, but as surface rivers easily reach $1.0\,\mathrm{m\,s^{-1}}$, we take this as an upper limit (Fig. 3).

To summarize, the contribution of friction to the energy available for basal melting may account for at least $\sim 200\,\mathrm{mW\,m^{-2}}$, with the potential to be by far larger based on the assumptions we made.

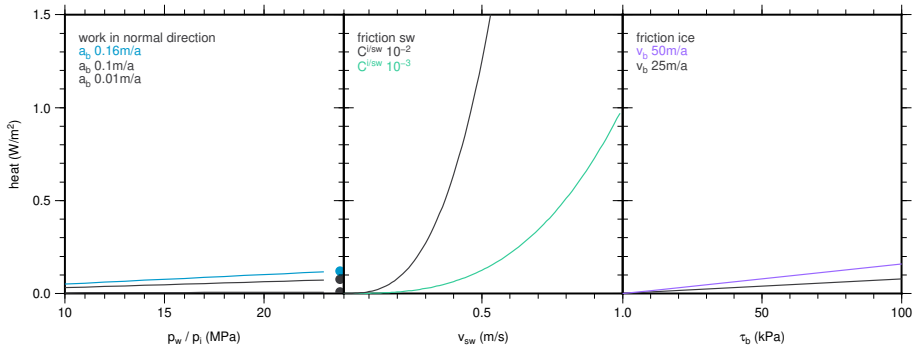

Figure 3. Magnitude of terms in the energy jump condition at the ice base. Contribution of work of surface forces in normal direction (left panel) and tangential direction (middle and right panels). The friction on the subglacial water and ice side are shown in the middle and right panel, respectively.

In particular, the jump in the tangential component (friction) has the potential to govern the heat budget, depending on flow speeds in subglacial water and roughness of the ice base, as can be seen in Fig. 3. However, assuming the geothermal heat flux to be in the order of $\mathcal{O}(q_\mathrm{geo}) \approx 0.25\,\mathrm{W\,m^{-2}}$ demonstrates that the key player in facilitating such high melt rates is the subglacial water system. Implications of large basal melting is predominantly its effect on sliding via the effective normal

https://doi.org/10.5194/tc-2021-37
Preprint. Discussion started: 2 February 2021

pressure. Considering sliding to be the dominant part of ice stream motion, large basal melt rates are also plausible in the respect that the subglacial hydrological system needs to be sustained over time and hence creep closure of cavities or conduits needs to be balanced by melting.

Future measurements at EastGRIP after successful completion will shed more light onto the sliding speed and may also provide more information on the characteristics of the subglacial hydrological system. This will enable the community to put our melt rate estimates into further context.

5 Conclusions

We estimated annual mean basal melt rates at the EastGRIP drill site from time series of high-precise phase-sensitive radar measurements. We derived the change in the measured ice thickness, thinning from firn densification occurring below the instrument and the vertical strain in the upper 1450 m of the roughly 2668 m thick ice. Three different scenarios for vertical strain distribution were used to to quantify a plausible range of dynamic thinning. Thus, we derived a range of melt rates from 0.16 to $0.22\,\mathrm{m\,a^{-1}}$. We are aware that these melt rates require an extremely large amount of heat that we suggest to arise from the subglacial water system and the geothermal heat flux. However, these melt rates are based on measurements with a modern ice penetrating radar whose penetration depth is limited due to transmitting power. Thus, no assumptions on past accumulation rates or other uncertainties in age reconstruction are involved. Our major uncertainty is the vertical strain in the lower part of the ice stream. This could be overcome if a more powerful radar with a similar vertical resolution could be operated autonomously over several months which we want to encourage herewith.

Code availability. Own developed MATLAB routines for ApRES processing are available from the corresponding author on.

Data availability. Raw data of the ApRES measurements are submitted to the World Data Center PANGAEA.

https://doi.org/10.5194/tc-2021-37
Preprint. Discussion started: 2 February 2021

The Cryosphere Discussions
Open Access
EGU

Appendix A: Additional figures of ApRES processing

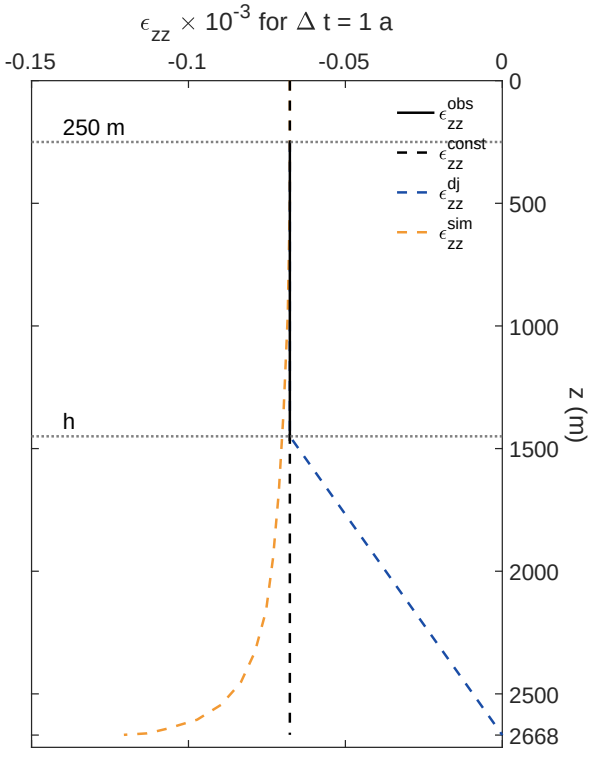

Figure A1. Observed vertical strain distribution (solid line) and different extensions to the ice base (dashed lines) for three scenarios based on a constant, a Dansgaard–Johnsen (Dansgaard and Johnsen, 1969) and a simulated (Rückamp et al., 2020) distribution.

https://doi.org/10.5194/tc-2021-37
Preprint. Discussion started: 2 February 2021

The Cryosphere Discussions
Open Access
EGU

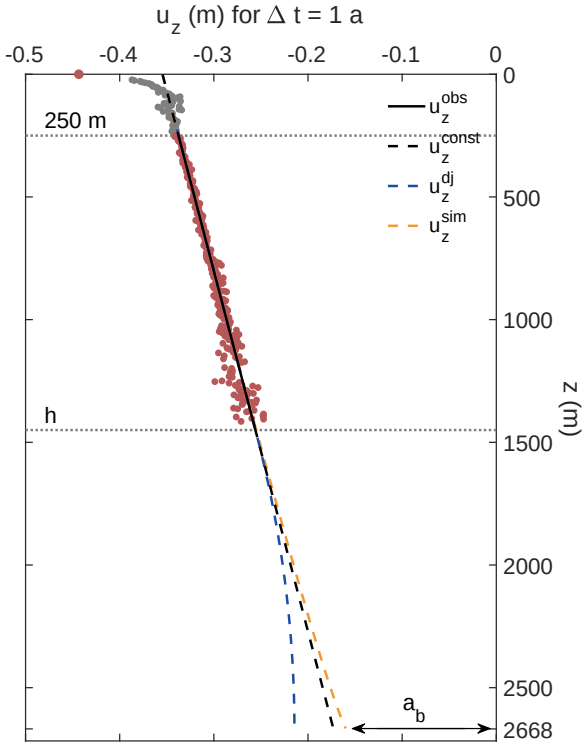

Figure A2. Derived vertical displacements u_z of the surface and selected internal layers referenced to the ice bed from 2018/19 ApRES time series. Derived displacements used for melt rate estimations are marked by red dots and of layers within the firn by gray dots. The estimated displacements between a depth of $250\,\mathrm{m}$ and h are used to calculate a linear fit (solid black line) which gradient is the vertical strain. Extrapolations to the bottom are shown by the dashed lines. The offset at the ice bed is caused by basal melting and the difference between the surface intercept of the linear fit and the derived surface displacement is the firn compaction.

Author contributions. O.Z., A.H. conducted part of the field study. O.Z. processed the ApRES data and estimated the resulting basal melt rates. A.H. has designed the study and conducted the analysis of the energy jump condition. O.Z. and A.H. discussed the basal melt rate distribution and time series. O.Z. and A.H. wrote the manuscript jointly.

Competing interests. The authors declare that they have no conflict of interest.

https://doi.org/10.5194/tc-2021-37
Preprint. Discussion started: 2 February 2021

Acknowledgements. Data has been acquired at the EGRIP camp that kindly hosted this activity as an associate project. EGRIP is directed and organized by the Centre for Ice and Climate at the Niels Bohr Institute, University of Copenhagen. It is supported by funding agencies and institutions in Denmark (A. P. Møller Foundation, University of Copenhagen), USA (US National Science Foundation, Office of Polar Programs), Germany (Alfred Wegener Institute, Helmholtz Centre for Polar and Marine Research), Japan (National Institute of Polar Research and Arctic Challenge for Sustainability), Norway (University of Bergen and Bergen Research Foundation), Switzerland (Swiss National Science Foundation), France (French Polar Institute Paul-Emile Victor, Institute for Geosciences and Environmental research) and China (Chinese Academy of Sciences and Beijing Normal University). We like to thank Johanna Kerch, Sepp Kipfstuhl and Daniel Steinhage for their support in the deployment and the dismount of the measuring device. We are grateful for discussions with Thomas Kleiner and Martin Rückamp (AWI) and Ralf Greve (ITLS, Japan) on vertical strain-rates and our results.

https://doi.org/10.5194/tc-2021-37
Preprint. Discussion started: 2 February 2021

References

Alley, R. B., Pollard, D., Parizek, B. R., Anandakrishnan, S., Pourpoint, M., Stevens, N. T., MacGregor, J. A., Christianson, K., Muto, A., and Holschuh, N.: Possible Role for Tectonics in the Evolving Stability of the Greenland Ice Sheet, Journal of Geophysical Research: Earth Surface, 124, 97–115, https://doi.org/10.1029/2018JF004714, 2019.

Brennan, P. V., Lok, L. B., Nicholls, K., and Corr, H.: Phase-sensitive FMCW radar system for high-precision Antarctic ice shelf profile monitoring, IET Radar, Sonar & Navigation, 8, 776–786, https://doi.org/10.1049/iet-rsn.2013.0053, 2014.

Christianson, K., Peters, L. E., Alley, R. B., Anandakrishnan, S., Jacobel, R. W., Riverman, K. L., Muto, A., and Keisling, B. A.: Dilatant till facilitates ice-stream flow in northeast Greenland, Earth and Planetary Science Letters, 401, 57–69, https://doi.org/10.1016/j.epsl.2014.05.060, 2014.

Dansgaard, W. and Johnsen, S.: A flow model and a time scale for the ice core from Camp Century, Greenland, Journal of Glaciology, 8, 215–223, https://doi.org/10.3189/S0022143000031208, 1969.

Fahnestock, M., Bindschadler, R., Kwok, R., and Jezek, K.: Greenland Ice Sheet Surface Properties and Ice Dynamics from ERS-1 SAR Imagery, Science, 262, 1530–1534, https://doi.org/10.1126/science.262.5139.1530, 1993.

Fahnestock, M. A., Abdalati, W., Joughin, I., Brozena, J., and Gogineni, P.: High geothermal heat flow, basal melt, and the origin of rapid ice flow in central Greenland, Science, 294, 2338–2342, https://doi.org/10.1126/science.1065370, 2001a.

Fahnestock, M. A., Joughin, I., Scambos, T. A., Kwok, R., Krabill, W. B., and Gogineni, S.: Ice-stream-related patterns of ice flow in the interior of northeast Greenland, Journal of Geophysical Research: Atmospheres, 106, 34 035–34 045, https://doi.org/10.1029/2001JD900194, 2001b.

Franke, S., Jansen, D., Beyer, S., Neckel, N., Binder, T., Paden, J., and Eisen, O.: Complex basal conditions and their influence on ice flow at the onset of the Northeast Greenland Ice Stream, Journal of Geophysical Research: Earth Surface, n/a, e2020JF005 689, https://doi.org/10.1029/2020JF005689.

Fujita, S., Matsuoka, T., Ishida, T., Matsuoka, K., and Mae, S.: A summary of the complex dielectric permittivity of ice in the megahertz range and its applications for radar sounding of polar ice sheets, in: Physics of ice core records, pp. 185–212, Hokkaido University Press, 2000.

Goelzer, H., Nowicki, S., Edwards, T., Beckley, M., Abe-Ouchi, A., Aschwanden, A., Calov, R., Gagliardini, O., Gillet-Chaulet, F., Golledge, N. R., et al.: Design and results of the ice sheet model initialisation initMIP-Greenland: An ISMIP6 intercomparison, The Cryosphere, 12, 1433–1460, https://doi.org/10.5194/tc-12-1433-2018, 2018.

Greve, R. and Blatter, H.: Dynamics of Ice Sheets and Glaciers, Springer Science & Business Media, https://doi.org/10.1007/978-3-642-03415-2, 2009.

Hvidberg, C. S., Grinsted, A., Dahl-Jensen, D., Khan, S. A., Kusk, A., Andersen, J. K., Neckel, N., Solgaard, A., Karlsson, N. B., Kjær, H. A., et al.: Surface velocity of the Northeast Greenland Ice Stream (NEGIS): assessment of interior velocities derived from satellite data by GPS, The Cryosphere, 14, 3487–3502, https://doi.org/10.5194/tc-14-3487-2020, 2020.

Joughin, I., Fahnestock, M., MacAyeal, D., Bamber, J. L., and Gogineni, P.: Observation and analysis of ice flow in the largest Greenland ice stream, Journal of Geophysical Research: Atmospheres, 106, 34 021–34 034, https://doi.org/10.1029/2001JD900087, 2001.

Joughin, I., Smith, B. E., and Howat, I. M.: A complete map of Greenland ice velocity derived from satellite data collected over 20 years, Journal of Glaciology, 64, https://doi.org/10.1017/jog.2017.73, 2018.

https://doi.org/10.5194/tc-2021-37
Preprint. Discussion started: 2 February 2021

Khan, S. A., Kjær, K. H., Bevis, M., Bamber, J. L., Wahr, J., Kjeldsen, K. K., Bjørk, A. A., Korsgaard, N. J., Stearns, L. A., Van Den Broeke, M. R., et al.: Sustained mass loss of the northeast Greenland ice sheet triggered by regional warming, Nature Climate Change, 4, 292–299, https://doi.org/10.1038/nclimate2161, 2014.

MacGregor, J. A., Fahnestock, M. A., Catania, G. A., Aschwanden, A., Clow, G. D., Colgan, W. T., Gogineni, S. P., Morlighem, M., Nowicki, S. M., Paden, J. D., et al.: A synthesis of the basal thermal state of the Greenland Ice Sheet, Journal of Geophysical Research: Earth Surface, 121, 1328–1350, https://doi.org/10.1002/2015JF003803, 2016.

Martos, Y. M., Jordan, T. A., Catalán, M., Jordan, T. M., Bamber, J. L., and Vaughan, D. G.: Geothermal heat flux reveals the Iceland hotspot track underneath Greenland, Geophysical research letters, 45, 8214–8222, https://doi.org/10.1029/2018GL078289, 2018.

Mouginot, J., Rignot, E., Scheuchl, B., Fenty, I., Khazendar, A., Morlighem, M., Buzzi, A., and Paden, J.: Fast retreat of Zachariæ Isstrøm, northeast Greenland, Science, 350, 1357–1361, https://doi.org/10.1126/science.aac7111, 2015.

Nicholls, K. W., Corr, H. F., Stewart, C. L., Lok, L. B., Brennan, P. V., and Vaughan, D. G.: A ground-based radar for measuring vertical strain rates and time-varying basal melt rates in ice sheets and shelves, Journal of Glaciology, 61, 1079–1087, https://doi.org/10.3189/2015JoG15J073, 2015.

Rignot, E. and Mouginot, J.: Ice flow in Greenland for the international polar year 2008–2009, Geophysical Research Letters, 39, https://doi.org/10.1029/2012GL051634, 2012.

Rogozhina, I., Petrunin, A. G., Vaughan, A. P., Steinberger, B., Johnson, J. V., Kaban, M. K., Calov, R., Rickers, F., Thomas, M., and Koulakov, I.: Melting at the base of the Greenland ice sheet explained by Iceland hotspot history, Nature Geoscience, 9, 366–369, https://doi.org/10.1038/ngeo2689, 2016.

Rückamp, M., Goelzer, H., and Humbert, A.: Sensitivity of Greenland ice sheet projections to spatial resolution in higher-order simulations: the Alfred Wegener Institute (AWI) contribution to ISMIP6 Greenland using the Ice-sheet and Sea-level System Model (ISSM), The Cryosphere, 14, 3309–3327, https://doi.org/10.5194/tc-14-3309-2020, 2020.

Smith-Johnsen, S., de Fleurian, B., Schlegel, N., Seroussi, H., and Nisancioglu, K.: Exceptionally high heat flux needed to sustain the Northeast Greenland Ice Stream, The Cryosphere, 14, 841–854, https://doi.org/10.5194/tc-14-841-2020, https://tc.copernicus.org/articles/14/841/2020/, 2020.

Stewart, C. L., Christoffersen, P., Nicholls, K. W., Williams, M. J., and Dowdeswell, J. A.: Basal melting of Ross Ice Shelf from solar heat absorption in an ice-front polynya, Nature Geoscience, 12, 435–440, https://doi.org/10.1038/s41561-019-0356-0, 2019.

Vaňková, I., Nicholls, K. W., Corr, H. F., Makinson, K., and Brennan, P. V.: Observations of tidal melt and vertical strain at the Filchner-Ronne Ice Shelf, Antarctica, Journal of Geophysical Research: Earth Surface, 125, e2019JF005 280, https://doi.org/10.1029/2019JF005280, 2020.